Eur. J. Mineral.
2006, **18**, 845-853

Iron (hydr)oxide nanocrystals in *raw* and *burnt* sienna pigments

ANDREA MANASSE* & MARCELLO MELLINI
Dipartimento di Scienze della Terra, Università degli Studi di Siena, Via del Laterino 8, I-53100, Siena, Italy

Abstract: The mineral pigments *raw sienna* and *burnt sienna*, known as bolar earths, mostly consist of iron (hydr)oxides; the two pigments, yellow and red-brown respectively, differ for thermal processing of the raw material.
Sixteen bolar earth samples from a quarry in Monte Amiata and from the Accademia dei Fisiocritici Museum were investigated by XRD, SEM-EDS, TEM-EDS, thermal treatment, TG/DTA and DRIFT.

Raw sienna is yellow to brown and prevalently contains goethite. *Burnt sienna* is red and consists of hematite obtained by dehydration of goethite at around 270°C. Chemical analyses show dominant Fe_2O_3 (53.5-71.5 wt.%), with minor SiO_2 (3.0-24.7 wt.%) and Al_2O_3 (0.8-7.1 wt.%). A very high arsenic content characterizes all the samples (with a mean of 5.6 wt.% As_2O_5). Goethite and hematite occur as finely dispersed nanocrystals, respectively 2-10 nm and 10-40 nm in size. They are enclosed in a minor amorphous silica matrix, with arsenic adsorbed on the iron (hydr)oxide nanoparticles. Due to its high arsenic content, the ochre used to produce *raw* and *burnt sienna* is an important example of an effective natural sink for arsenic.

Key-words: *raw* and *burnt* sienna, goethite, hematite, arsenic.

Introduction

Clay earth pigments generally consist of naturally-occurring metal oxide or hydroxide colorants dispersed in small quantities in a clay base. They have been used in painting since Palaeolithic times (15,000 years ago), as the cave paintings of Altamira (Spain) and Lescaux (France) testify (Pomies *et al.*, 1999). The technological processes used to produce pigments have been documented through the centuries by many authors: *Theophrast*, *Vitruvius*, *Pliny the Elder* in Antiquity, *Heraclius* ("De coloribus et artibus Romanorum") and *Cennino Cennini* ("Il libro dell'arte") in the Middle Ages, *Vannoccio Biringuccio* ("De La Pirotechnia") and *Cipriano Piccolpasso* ("Li tre libri sull'arte del vasaio") in the Renaissance.

In Italy, deposits of clay earth pigments occurred in the ochreous sediments of southern Tuscany (Monte Amiata, near Siena), which were exploited for the production of two pigments known as *raw sienna* and *burnt sienna* ("*Terra di Siena naturale*" and "*Terra di Siena bruciata*" in Italian). These names evidently refer to the provenance and technological processing of the earth, but are now used for all pigments with similar tinting properties.

Widely exploited for industrial commerce in the 19th and 20th centuries (up to 50,000 tons; Fei, 1997), the *sienna* pigments were largely used by the most important Tuscan artists of the Middle Ages and the Renaissance (*e.g.*, Duccio di Buoninsegna and Ambrogio Lorenzetti). In contrast to other clay earth pigments, *raw* and *burnt sienna* are bright colours with a high coating efficiency (Moretti, 1937; Harley, 1982; Scarzella & Natale, 1989).

Raw sienna is generally divided into *yellow earths* and *brown boles*, plus intermediate yellow to brown *bolar earths ("terre bolari"* in Italian).

After extraction from the quarry, yellow earths were dried in the sun for several days before grinding and then trading; brown boles were kept closed in shelters for a longer period (Giannetti, 1873). After heating, the raw bolar earths changed colour from light yellow to pale red and from brown to dark red.

Yellow earths and brown boles deposited as ochreous lacustrine sediments within small basins in the Middle Pleistocene trachydacitic formation of the Monte Amiata volcanic area (Ferrari *et al.*, 1996; Fig. 1). They resulted from the low-temperature, hydrothermal solute-rich fluids subsequent to the late volcanic stage. These iron-rich fluids fed small streams which flowed into the basin (as first noted by Gasperini, 1906).

Several factors, such as pH and water temperature, redox conditions, and biological and chemical activity, regulated the accumulation of the iron-rich stratified deposits, which are up to 13 meters thick. The dominant role of biological and/or chemical controls in the precipitation of bolar earths has been widely discussed in the past. Based on chemical analyses and direct observation of micro-organisms such as *Bacillus ferrooxidans* (originally

*E-mail: manasse@unisi.it

0935-1221/06/0018-0845 $ 4.05
DOI: 10.1127/0935-1221/2006/0018-0845

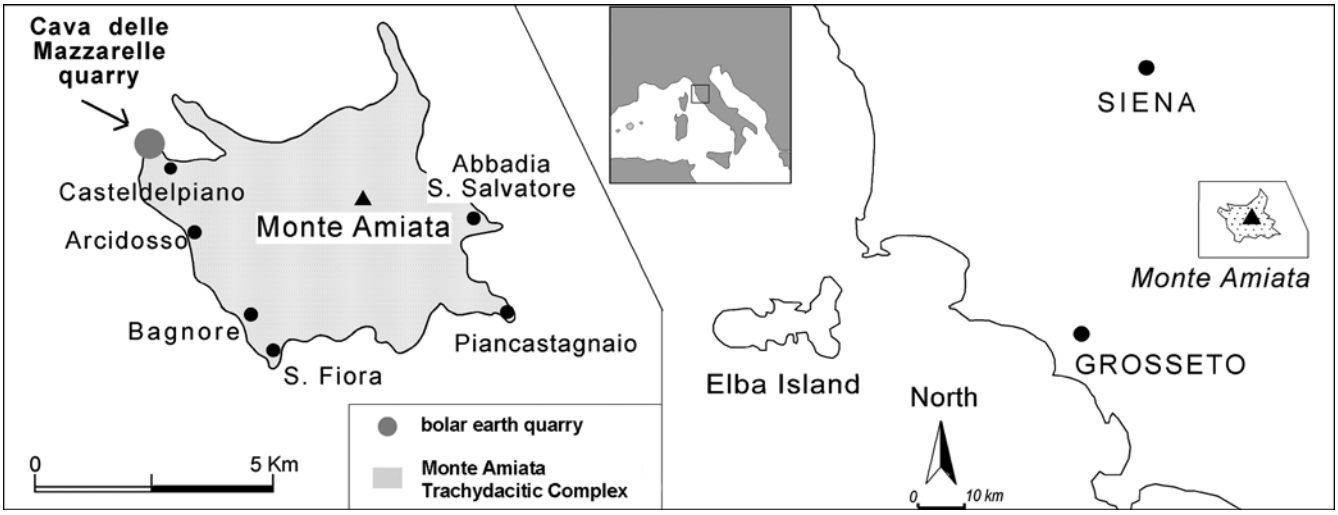

Fig. 1. Schematic map of the Monte Amiata district indicating the Cava delle Mazzarelle quarry.

called "ferrigenus") or *Beggiatoaceae*, Lotti (1910) and Manasse (1915) suggested the presence of coupled chemical and biological controls. Biologically-controlled oxidation was thought to promote the precipitation of ferric hydroxide, possibly as an amorphous phase later transformed into crystalline iron hydroxide. These early works were the first to consider biomineralization processes.

Due to the widespread use of *raw* and *burnt sienna* in ancient and modern painting, we now present their mineralogical and chemical characterization, with the aim to understand their peculiar features.

Experimental

Four specimens (labelled **TG**) were sampled in the abandoned Cava delle Mazzarelle quarry (Fig. 1), from which bolar earths were previously extracted to produce pigments. In 2003, the bolar earths still occurred as pockets containing almost pure yellow to brown ochreous sediments; they are now mostly flooded by a recently built artificial basin. Twelve more samples (**TB**) collected in 1867 come from the historic Pantanelli collection of the Natural History Museum of the Accademia dei Fisiocritici of Siena. The collection consists of 60 samples (loose powders or pressed bricks approximately 15 cm long) representing the whole range of yellow-red colours produced in the 19th century. The selected TG and TB samples (Table 1) cover this range.

Mineral phases were determined through X-ray powder diffraction (XRPD). Data were collected using an automated Philips PW1710 Bragg-Brentano diffractometer equipped with a post-diffraction monochromator using Cu$K\alpha$ radiation (γ = 1.5418 Å) and operating at a scan speed of 1.2°/min in the 5 to 70° 2θ range.

Due to the small quantity of available material, we chose to obtain chemical compositions by energy dispersive spectrometry (EDS) using both scanning (SEM) and transmission (TEM) electron microscopy.

SEM-EDS was performed using a Philips XL30, operating at 20 kV and equipped with an EDAX-DX4 spectrometer. EDS analyses (counting rates close to 2000-2500 cps) were performed using a beam raster 50 × 50 μm wide; mean value of five analyses is reported for each sample. Raw data were corrected using ZAF approach. Analytical precision, checked by repeated analyses, was better than 0.5 wt. % for major elements (on the absolute value) and better than 20 % relative for minor elements (*i.e.*, those with contents ranging from 0.3 wt.% up to 3-5 wt.%).

The morphology and size of goethite and hematite nanocrystals were determined by a JEOL 2010 TEM, equipped with a semistem system allowing the acquisition of X-ray maps and an ultra-thin window energy dispersive spectrometer (EDS-ISIS Oxford). TEM-EDS analyses were obtained using large beam spots (approximately 100 nm in diameter), and counting rate between 500 and 1000 cps; TEM specimens were prepared by depositing the powders on Cu grids, covered with a supporting carbon film.

Step-heating experiments were used to characterize the thermally-induced phase transitions. The goethite-hematite transformation was further investigated by thermogravimetric analysis using a SEIKO 5200 TG/DTA instrument. After dehumidification at 25°C for 10 min. under helium, TG/DTA analyses were performed from room temperature to 800°C at a heating rate of 10°C/min.

Quantitative colour measurements for thermally-treated specimens were obtained using a Minolta CR-200 colorimeter, with reference to the CIE-$L^*a^*b^*$ system of colour measurement (Cheinost & Schwertmann, 1999). The system defines colours by the Cartesian axes a^* (red-green) and b^* (yellow-blue); a third axis normal to a^* and b^* defines the lightness, L^*.

Infra-red spectrometry was performed using a NEXUS FTIR-spectrometer, operating in Diffuse Reflectance mode (DRIFT). Yellow and red samples were previously dried for three days at 35°C. Spectra were recorded between 4000 and 400 cm^{-1} using powders diluted in KBr.

Table 1. Bolar earths from the Cava delle Mazzarelle quarry (**TG**) and from the 19th century Accademia dei Fisiocritici Museum (**TB**).

					Relative intensities				FWHM			
TG	**Colour**	**Goethite**	**Hematite**	**Others**	**1 1 0**	**1 3 0**	**1 1 1**	**2 2 1**	**1 1 0**	**1 3 0**	**1 1 1**	**2 2 1**
1	pale yellow	xx			100	34	70	33	0.3	0.5	0.5	0.2
2	pale yellow	xx			100	25	61	32	0.4	0.6	0.5	0.3
3	dark yellow	xxx		quartz	100	42	88	28	0.5	0.5	0.2	0.5
4	brown	xxx			100	47	101	48	0.4	0.5	0.6	0.6
TB												
3469	dark brown	xx			100	16	133	45	1.3	1.0	0.7	0.8
3474	dark brown	x		sheet silicates	100	42	384	187	0.8	1.0	0.6	0.8
3475	light brown	xx		sheet silicates	100	39	125	46	1.0	0.8	0.3	1.1
3477	dark yellow	xxx			100	20	166	70	0.6	1.0	0.6	0.6
3479	dark yellow	xxx		sheet silicates	100	49	96	33	0.3	0.4	0.4	0.8
3480	dark yellow	xxx			100	48	188	66	0.7	1.3	0.2	0.7
3488	dark yellow	xxx			100	43	106	36	0.3	0.5	0.3	0.6
3547	yellow	x		feldspars	n.d	n.d	n.d	n.d	n.d	n.d	n.d	n.d
TB					**1 0 4**	**1 1 0**	**0 2 4**	**1 1 6**	**1 0 4**	**1 1 0**	**0 2 4**	**1 1 6**
3497	dark brown		x		100	44	25	71	1.0	0.5	1.1	1.1
3509	dark red		xxx		100	85	24	77	0.5	0.3	1.1	0.4
3517	dark red		xxx		100	97	28	54	0.4	0.5	0.8	0.5
3522	dark brown		xxx		100	86	33	42	0.2	0.5	0.4	0.4

Colours, mineral phases and amount (x = low; xxx = abundant), relative intensities and Full Width at Half Maximum (FWHM) are reported for selected peaks.

Results

X-ray powder diffraction

The TG quarry samples consist almost exclusively of goethite (Table 1); the TB museum samples consist of goethite (with minor clay minerals) or hematite. Goethite occurs in yellow earths, while hematite occurs in red samples (TB3509, TB3517); intermediate colours are associated with either goethite (TB3469, TB3474, TB3475) or hematite (TB3497, TB3522). The low peak/background ratio generally hampers the identification of minor phases, where present.

Both goethite and hematite XRPD patterns show weak, broad peaks, as detailed in Table 1 for their four major peaks.

Step-heating

Four samples from "Cava delle Mazzarelle", ranging from yellow to dark-brown, were treated at 200, 250, 300, 350, 400 and 800°C under oxidizing conditions and at a heating rate of 10°C/min. They changed colour in the 250-300°C range (Table 2). The CIE-*L*a*b** coordinates of the different burnt products demonstrate that the darkest red ones (*e.g.* TG4) derive from thermal treatment of brown starting materials.

XRPD of natural and heated samples (Fig. 2) confirms that the goethite-hematite transformation occurs in the 250-300°C range, with the major hematite peaks progressively substituting those of goethite. This is in agreement with Cornell & Schwertmann (2003), who report yellow-to-red conversion of earth pigments by thermal treatment at temperatures close to 270°C.

The diffraction pattern of newly formed hematite exhibits selective peak broadening and biased intensities, as reported in previous works (Pomies *et al.*, 1998; Gualtieri & Venturelli, 1999; Walter *et al.*,2001). For instance, the 110 peak is narrow (FWHM = 0.5), while the 104 peak is broad (FWHM = 0.9); although 110 is expected

Table 2. Colour data for natural and heated ochres.

sample	**natural**	**200°C**	**250°C**	**300°C**	**350°C**	**400°C**
TG 1	**pale yellow**	**pale yellow**	**orange-yellow**	**orange**	**orange**	**orange**
a*	11.6	12.0	17.0	28.8	28.7	28.8
b*	45.1	44.9	41.2	36.0	35.1	35.1
L*	64.2	63.4	57.3	43.6	42.2	42.4
TG 2	**pale yellow**	**pale yellow**	**orange-yellow**	**orange**	**orange**	**orange**
a*	11.8	12.2	18.8	29.2	29.5	29.4
b*	46.7	46.1	41.5	37.2	37.3	36.6
L*	62.7	61.8	54.4	41.9	42.0	41.1
TG 3	**dark yellow**	**dark yellow**	**orange**	**red**	**red**	**red**
a*	14.7	15.3	22.2	29.3	29.2	27.7
b*	50.3	48.1	40.6	31.3	30.7	29.9
L*	56.1	53.5	44.7	33.5	32.7	32.1
TG 4	**brown**	**brown**	**dark orange**	n.d.	n.d.	**dark red**
a*	14.8	15.5	20.5			21.2
b*	39.0	37.5	24.6			17.0
L*	42.7	41.5	30.1			22.0

Measurements were carried out on powdered materials. Colour is expressed using the CIE-*L*a*b** system. The darkest red hues derive from brown starting materials.

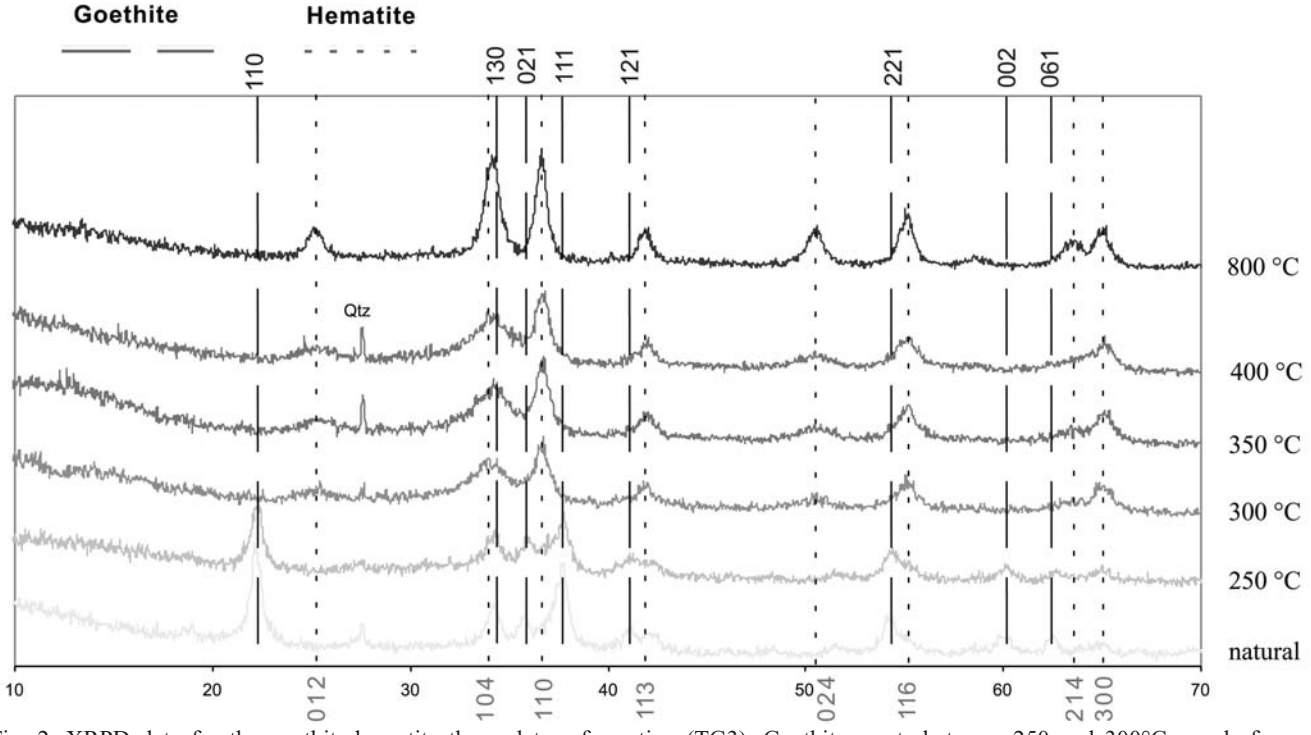

Fig. 2. XRPD data for the goethite-hematite thermal transformation (TG3). Goethite reacts between 250 and 300°C; newly-formed hematite exhibits selective peak broadening that progressively disappears at high temperatures (800°C).

to be weaker than 104, the opposite is true for early-formed hematite, at least up to 400°C. Peak broadening and biased intensities progressively disappear at higher temperatures (800°C) as a result of thermal annealing.

SEM-EDS data

TB samples are rich in Fe_2O_3 (53.5-67.3 wt.%), with variable SiO_2 (3.0-24.7 wt.%) and Al_2O_3 (0.8-7.1 wt.%)

Table 3. SEM-EDS data (wt.%; mean value) for yellow, red and bolar earths from the Accademia dei Fisiocritici (**TB**) and the Cava delle Mazzarelle quarry (**TG**); a mean H_2O content of 15 wt.% was assumed based on thermogravimetry.

TB	**3469** d. b.	**3474** d. b.	**3475** l. b.	**3477** d. y.	**3479** d. y.	**3480** d. y.	**3488** d. y.	**3547** y.	**3497** d. b.	**3509** d. r.	**3517** d. r.	**3522** d. b.
As_2O_5	10.9	10.4	4.3	7.3	2.3	7.1	0.7	7.7	10.3	7.8	2.8	7.4
Al_2O_3	2.2	0.9	0.9	1.1	5.9	1.0	0.9	1.3	1.0	0.9	8.3	1.0
SiO_2	3.0	16.2	22.7	15.5	17.7	6.0	24.7	15.9	17.8	10.8	15.5	25.7
CaO	1.7	2.4	1.0	1.6	0.4	0.9	0.4	1.4	2.9	1.0	0.8	2.4
MnO	0.7	0.3	0.3	0.3	0.2	0.0	0.0	0.9	0.2	0.0	0.3	0.3
Fe_2O_3	66.6	54.8	55.8	58.3	58.0	69.5	58.2	57.5	67.7	79.2	70.9	63.0
$[H_2O]$	15.0	15.0	15.0	15.0	15.0	15.0	15.0	15.0				

TG	**1** p. y.	**2** p. y.	**3** d. y.	**4** b.
As_2O_5	-	-	0.8	3.3
Al_2O_3	0.9	0.9	1.5	1.0
SiO_2	70.2	64.0	11.2	9.9
CaO	-	-	0.0	0.4
MnO	-	-	0.0	0.0
Fe_2O_3	13.9	20.1	71.5	70.4
$[H_2O]$	15.0	15.0	15.0	15.0

Manasse (1915)	yellow earth	bole dark yellow	bole dark yellow	bole brown	bole dark brown
As_2O_5	0.6	0.7	1.0	2.2	9.0
Al_2O_3	0.4	0.4	0.4	0.6	0.9
SiO_2	14.6	14.3	12.9	11.6	13.0
CaO	0.2	0.1	0.2	0.3	1.2
MnO	-	-	0.1	0.2	0.6
Fe_2O_3	65.7	65.9	66.0	64.6	52.5
H_2O	18.2	18.5	19.0	20.9	23.0

Data by Manasse (1915) is reported for comparison. Legend: d. b. = dark brown, l. b. = light brown, d. y. = dark yellow, y. = yellow, d. r. = dark red, p. y. = pale yellow, b. = brown.

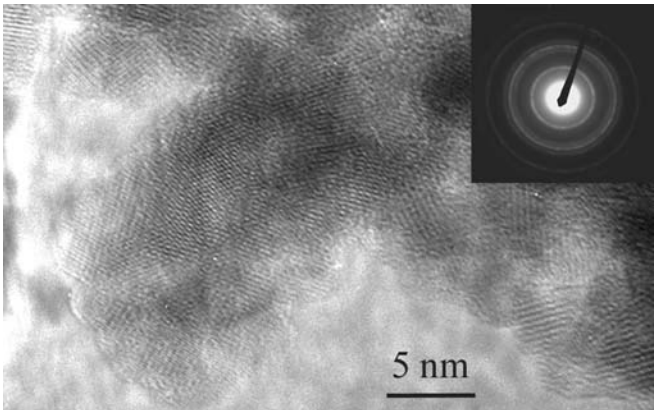

Fig. 3. High resolution TEM image of fine goethite nanoparticles 2-10 nm in size (sample TG4). SAED pattern (with diffuse rings) in the inset.

contents. Very high arsenic contents are common to all the samples, with a mean value of 5.6 wt. % and maximum value of 10.9 wt. % in TB3469 (calculated as As_2O_5).

Our data match the chemical compositions obtained by Manasse (1915) for "*sienna earths*" quarried at Cava delle Mazzarelle, with As contents up to 9.0 wt.% (Table 3). Manasse (1915) suggested that the higher the arsenic the darker the sample; our results do not support this finding, since brown samples may contain less arsenic than yellow ones (TB3475 vs. TB3547, in particular).

Data on natural yellow earths from "Cava delle Mazzarelle" (**TG**) are similar to those on **TB** samples in the case of TG3 and TG4. In contrast, TG1 and TG2 have decidedly higher silica contents. Higher arsenic contents characterize the iron-rich samples (up to 3.3 wt.% in TG4).

SEM was unable to identify individual particles, since the sample is a very fine aggregate of particles smaller than the available resolution.

TEM investigation

TEM investigation was carried out on two natural ochres (TG3 and TG4, with 0.8 and 3.3 wt.% As_2O_5, respectively) and on two historical specimens (the goethite-bearing TB3469 and hematite-bearing TB3509, containing 10.9 and 6.7 wt.% As_2O_5 respectively). TG4 was also studied after thermal treatment (1 hour at 400°C).

Goethite ochres

At low magnification, the ochres appear as fine aggregates of iron hydroxide nanocrystals plus clay minerals with smectite-like composition. Tiny goethite nanoparticles 2 to 10 nm in diameter are resolved at very high magnification only (*e.g.*, > 5*10^5 ×) (Fig. 3). Lattice fringes are irregular and bent, with dominant lattice fringe spacing of 2-3 Å. The mutual lattice fringe orientation indicates randomly oriented particles; diffuse ring-shaped diffraction patterns (either selected area electron diffraction, SAED, or nanobeam diffraction) confirm the low crystallinity of goethite.

Table 4. TEM-EDS data (wt.%) for natural and heat-treated (TG4-400°C) ochres (goethite and hematite-bearing, respectively).

TB 3469	**# 1**	**# 2**	**# 3**	**# 4**	**# 5**	**average**
SiO_2	2.2	5.1	6.4	5.0	2.8	**4.3**
CaO	1.8	1.3	1.5	1.2	2.4	**1.6**
Fe_2O_3	70.2	71.1	68.9	73.2	69.6	**70.6**
As_2O_5	10.7	7.5	8.2	5.6	10.2	**8.4**
[H_2O]	15.0	15.0	15.0	15.0	15.0	**15.0**

TG 4	**# 1**	**# 2**	**# 3**	**# 4**	**average**
SiO_2	5.4	5.7	6.6	5.6	**5.8**
CaO	0.4	0.4	0.3	0.5	**0.4**
Fe_2O_3	76.4	76.2	75.4	76.7	**76.2**
As_2O_5	2.8	2.7	2.8	2.3	**2.6**
[H_2O]	15.0	15.0	15.0	15.0	**15.0**

TG 4 400°C	**# 1**	**# 2**	**# 3**	**# 4**	**average**
SiO_2	8.1	3.6	1.7	0.7	**3.5**
CaO	-	-	-	-	**-**
Fe_2O_3	89.3	94.2	95.6	96.4	**93.9**
As_2O_5	2.6	2.3	2.7	2.8	**2.6**

Data obtained using a 100 nm spot.

Arsenic contents (Table 4) are similar to those determined through SEM-EDS. No specific crystalline phase was detected for arsenic, which occurs dispersed throughout goethite. X-ray maps of nanosized goethite aggregates reveal that the distribution of arsenic closely matches that of iron (Fig. 4).

Hematite pigments

Hematite commonly occurs as acicular crystals up to 40 nm long in the 1867 TB3509 pigment (Fig. 5). The average arsenic content is close to 5 wt.%. Silica is present in the non-crystalline portion of the aggregate. Smectite-like minerals may occur.

The habit of hematite obtained by dehydration of goethite at 400°C (sample TG4) is different. Fine aggregates of iron oxides, with nanoparticles 5 to 10 nm in diameter, retain the morphology of the precursor goethite. The different habits and sizes may be explained by invoking a more prolonged thermal treatment of commercial product TB3509.

Thermal analyses

Thermogravimetric (Table 5) and differential thermal analyses (TG/DTA) of TG1, TG3, TG4 and TB3469 were completed to better characterize the goethite-hematite transformation.

Differential thermal analyses show two endothermic peaks below 100°C (*e.g.*, 60°C in Fig. 6) and 274°C. The first step, with a weight loss of 2.8-6.9 %, corresponds to loss of imbibition water. The main reaction at 274°C is due to the goethite-hematite transformation; weight loss

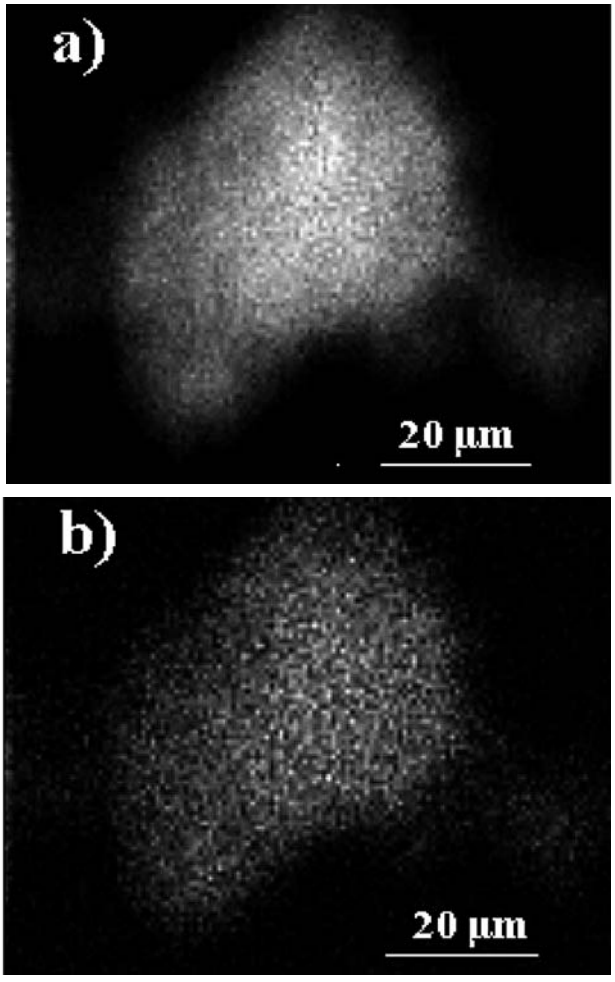

Fig. 4. X-ray maps of nanosized goethite aggregates. The distribution of arsenic (b) matches that of iron (a).

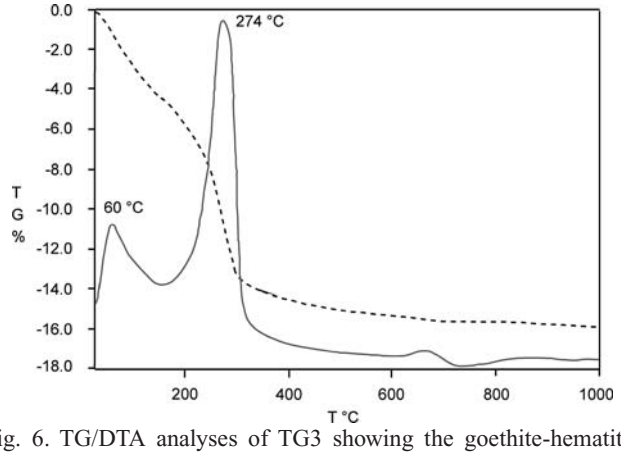

Fig. 6. TG/DTA analyses of TG3 showing the goethite-hematite transformation at 274°C.

Table 5. Successive weight losses obtained by TG/DTA analyses.

	< 100°C	200-300°C	300-600°C	Total
TG 1	2.8	2.0	0.5	5.3
TG 3	4.2	8.9	1.6	14.7
TG 4	5.7	8.3	1.4	15.3
TB 3469	6.9	8.0	1.2	16.0

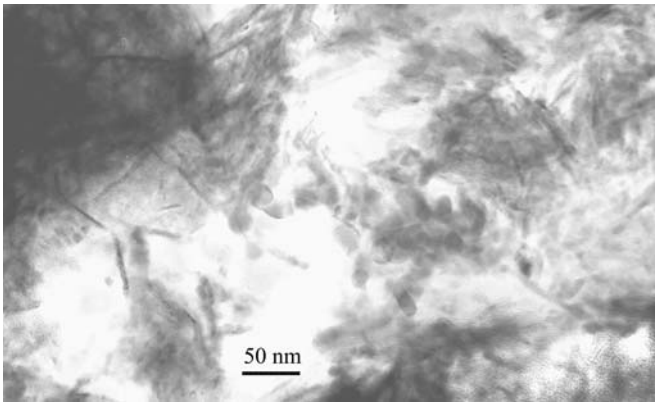

Fig. 5. TEM image of acicular hematite particles 5-40 nm in size in TB3509.

reaches 8.0-8.9 % in the samples richest in iron (TB3469, TG3, TG4). Only limited weight loss was observed after the main reaction.

No reactions due to further phase transformations were detected from TG/DTA analyses, thereby confirming XRPD and TEM-EDS results.

IR spectrometry

Diffuse Reflectance Infrared Fourier Transform (DRIFT) spectrometry on goethite-bearing TB3469, TG3 and TG4 ochres (Fig. 7a) show a very broad, asymmetric and strong hydroxyl stretching band at 3192 cm^{-1}. A hydroxyl bending band occurs at lower wavenumbers (at 1636-1637 cm^{-1}), followed by two narrow, intense hydroxyl deformation bands at 891-912 cm^{-1} and 796-797 cm^{-1}, respectively. The hydroxyl translation band occurs at 607 cm^{-1} for TG3 and at 619 cm^{-1} for TG4, whereas it is not resolved in TB3469. Octahedral Fe-O vibrations occur at low wavenumbers as broad peaks between 458 and 472 cm^{-1}. Yellow samples show another band at 1013-1036 cm^{-1} due to tetrahedral Si-O stretching.

IR spectra obtained for the TB3509 (Fig. 7b) and TB3517 hematite-bearing samples mostly show the Fe-O bands at low wavenumbers. However, a weaker broad band still occurs at 3367 and 3409 cm^{-1} (for TB3509 and TB3517, respectively), although with lower intensities than in yellow samples. This band indicates the persistence of hydroxyl and/or water.

IR results for yellow ochres well agree with experimental spectra obtained for synthetic goethite (Ruan *et al.*, 2002), although the Fe-O band at ~350-380 cm^{-1} was not verified because it was out of our spectral range.

Despite the high arsenic contents, no characteristic arsenate vibrations were identified. In agreement with findings by Myneni *et al.* (1998), tetrahedral As-O stretching vibrations occur between ~700 and ~800 cm^{-1}, depending on the occurrence of AsO_4^{3-} (solution, crystal or sorbed on mineral surfaces). These frequencies are masked by the intense hydroxyl deformation bands occurring in both goethite and hematite samples.

Discussion and conclusions

Pigment characteristics

The widespread, effective use of *raw* and *burnt sienna* in ancient and modern painting derives from their excellent coating power and tinting strength. These properties stem from the nanosize of the goethite and hematite crystals. In contrast to other earth pigments, the fact that the only mineral phases in these bolar earths are goethite or hematite further increases their tinting strength (Scarzella & Natale, 1989). These fine-grained pigments maintain their deep, bright colour even when mixed with other dispersing media. Our four TG specimens, originally sampled because of their yellow to brown colours, also show this property. Analytical data reveals that TG1 and TG2 are not true earth pigments but silica-rich sediments deeply coloured by minor goethite contents (13.9-20.1 wt.% Fe_2O_3).

Goethite and hematite yield weak, broad XRPD peaks and ring-shaped, diffuse electron diffraction patterns. Low crystallinity is due to either size (*i.e.,* particle dimensions of 2-10 nm and 10-40 nm for goethite and hematite, respectively) or internal disorder (evident in TEM images as irregular, bent lattice fringes). As previously observed (Scarzella & Natale, 1989; Cornell & Schwertmann, 2003), goethite crystals from lacustrine deposits are commonly nanosized. However, the crystallinity of quarry samples is greater than that of processed ones (*e.g*., sharper peaks and higher intensities). Natural samples were probably processed (*e.g*., by mechanical grinding or sedimentation fractionation) to obtain finer goethite or hematite crystals. Processing, which evidently aimed to achieve the best coating properties, unknowingly led to the selection of the smallest nanoparticles.

X-ray diffraction data reveal the presence of goethite in the raw bolar earths, and the presence of hematite in the red-coloured *burnt sienna* varieties. Although similar in particle size, *raw* and *burnt sienna* underwent different thermal processing. Whereas *raw sienna* was produced by simply drying the quarried material for several days, *burnt sienna* was obtained by dehydration of goethite at temperatures close to 270°C. Quantitative colorimetric determinations reveal a yellow-to-red variation in hue, corresponding to goethite-to-hematite dehydration, during heating in the 250-300°C range. The CIE-*L*a*b** coordinates remain constant above 300°C, with no further evolution of colour.

The low-temperature transformation of goethite leads to hematite with anomalous XRPD features (*i.e.*, selective peak broadening and biased peak heights; Helwig, 1997). Experimental data (this study; Pomies *et al.*, 1998; Gualtieri & Venturelli, 1999; Walter *et al*., 2001) show that selective broadening progressively decreases with temperature, and disappears at 800°C. This thermal annealing effect relates to the modified crystalline state of the newly formed hematite between 300 and 800°C. TEM observations reveal that low-temperature hematite occurs as needle-like particles, with a crystal habit directly inherited from the precursor goethite. We believe that both XRPD selective broadening and biased intensities result from the inequant habit of hematite. The several unit cells occurring along the [001] direction of hematite elongation determine the almost perfect diffraction pattern of crystals as far as the 00*l* reflections are concerned. Conversely, the *hk*0 reflections are largely imperfect because of the limited number of lattice translations.

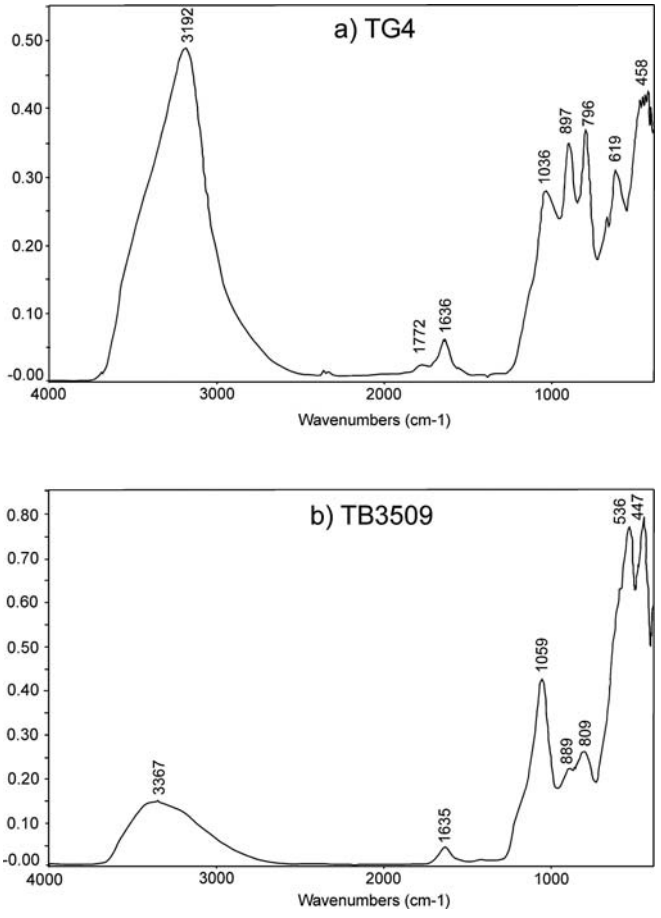

Fig. 7. DRIFT spectra of a) TG4 and b) TB3509 in the 4000-400 cm^{-1} region.

This behaviour is favoured by the slow recrystallization rate of hematite. While dehydration from goethite-to-hematite is easily accomplished at 270°C, hematite recrystallization continues until at least 800°C. Furthermore, both thermal analyses and infrared spectrometry indicate the possible persistence of hydroxyl and/or water, possibly hosted within residual porosity of early-formed hematite (Pomies *et al.*, 1998; Gualtieri & Venturelli, 1999; Walter *et al*., 2001; Cornell & Schwertmann, 2003). Alternatively, some hydrogen may be bonded to oxygen of the iron or arsenic coordination groups.

After the goethite-hematite transition, the colour does not change with heating. We therefore conclude that the darkness of pigments does not depend on heating but on the starting composition of the raw material. Manasse (1915) suggested that arsenic was responsible for dark earth pigments. However, our SEM-EDS results show the absence of such a straightforward relationship and suggest that the given yellow-to-brown colour results from the

complex interaction of several other parameters, such as crystallinity of iron (hydr)oxides, particle size, aggregation patterns, minor elements (*e.g.* manganese, arsenic or colloidal silica; Table 3) and organic matter. This conclusion is in agreement with previous studies (Cornell & Schwertmann, 2003), which emphasized the role of particle shape and manganese, alumina and organic matter contents. For example, they showed that goethite with different crystallinity (affecting the visible light adsorption spectra) or particle shapes (affecting the orientation towards the incident light) produced different mineral hues.

Arsenic adsorption

The high arsenic content in bolar earths (mean value of 5.6 wt.%) may strongly affect the environmental properties of goethite ochres. Arsenic (ubiquitous in water and soils) is potentially toxic to humans, with As (V) (dominant species under non-reducing conditions) less toxic than As (III) (Smedley & Kinniburgh, 2002). We now focus our attention on the adsorption of arsenic on earth pigments and on the possible role of goethite sediments as temporary traps for arsenic.

As for arsenic adsorption, we repeat that the distribution of arsenic in bolar earths closely follows that of iron in goethite and hematite, and that no segregated As-bearing phases were detected by XRPD or TEM-EDS. In agreement with many authors (Fuller *et al.*, 1993; Fendorf *et al.*, 1997; Cornell & Schwertmann, 2003), our data indicate As-adsorption on iron oxides and hydroxides. Infrared and extended X-ray absorption fine structure (EXAFS) spectroscopies (Waychunas *et al.*, 1993; Sun & Doner, 1996; Fendorf *et al.*, 1997; Grossl *et al.*, 1997; Sherman & Randall, 2003) indicate adsorption of arsenate on iron (hydr)oxides which form surface complexes by ligand exchange with hydroxyl groups at the mineral surface. Three different complexes (two bidentate and one monodentate) may form through this adsorption process. EXAFS studies of goethite have shown that the AsO_4 tetrahedra are linked by corner-sharing to pairs of FeO_6 octahedra, forming the so-called bidentate complex (Waychunas *et al.*, 1995; Sun & Doner, 1996; Manning *et al*., 1998, O'Reilly *et al*., 2001; Gao & Mucci, 2001). This adsorption mechanism leads to a negatively-charged outer shell capable of inhibiting the outward growth of hydroxide; nanosized goethite particles therefore arises as a surface poisoning effect. Alternatively, nanosized dimensions might be envisaged as resulting from the neutralising effect of the arsenate anions on the positively charged surfaces of the goethite colloid. When the isoelectric point is reached, As-adsorbing goethite nanoparticles flocculate from solution (Cornell & Schwertmann, 2003).

The very high arsenic content of bolar earths is closely linked to the nanosize of goethite particles. Indeed, all the iron (hydr)oxides species show an inverse correlation between particle size and specific surface area (Cornell & Schwertmann, 2003). The occurrence of goethite nanoparticles, observed under high-resolution TEM, results in a high number of surface functional groups that can interact with soluble species such as arsenate, thereby increasing their total adsorption.

Detailed, atomistic knowledge of As-adsorption by iron oxides and hydroxides is important to predict the long-term fate of As in sediments in different geochemical environments. The most important factor controlling As-adsorption is pH; optimal values are in the pH = 3-6 range, definitely lower than the point of zero charge of the sorbent (pH = 9 for goethite) (Dzombak & Morel, 1990; Fuller *et al.*, 1993; Sun & Doner, 1996; Manning *et al.*, 1998; Garcia-Sanchez *et al.*, 2002; Dixit & Hering, 2003; Antelo *et al.*, 2005). With increasing pH, arsenic retention rapidly decreases and its solubility and mobility increases.

Redox conditions are also important, because a reducing environment may transform As (V) into the more dangerous As (III) (Smedley & Kinniburgh, 2002). Lastly, the solubility and mobility of arsenic in the environment may also be controlled by other substances such as colloidal silica, other competitive ligands for similar sorption sites (phosphates, chromates, *etc*.), alumina and organic matter (Hingston *et al.*, 1971; Manning & Goldberg, 1996; Fendorf *et al.*, 1997; Grossl *et al.*, 1997; O'Reilly *et al.*, 2001; Hiemstra & Van Riemsdijk, 1999; Gao & Mucci, 2001; Gräfe *et al.*, 2001).

The Monte Amiata basins therefore seem to be ideal environments for the quantitative study of mechanisms by which a certain percent of arsenic is fixed within sediments. Unfortunately, some historic sites (such as the Cava delle Mazzarelle quarry) were first exhausted and later completely erased by remediation operations. Notwithstanding these difficulties, we believe that it would be important to undertake a detailed field survey to locate any persisting traces of arsenic sources and traps in the area. On one hand, these sites may contain examples of old, hopefully stabilized deposits, or of currently forming As-rich goethite deposits, thereby providing further insight into arsenic mobility. On the other hand, these sites may also allow the identification of possible natural arsenic bioremediation processes.

Acknowledgements : The authors are grateful to the Natural History Museum of the Accademia dei Fisiocritici of Siena for providing rare samples and photos for research purposes. Thanks to Cecilia Viti for reviewing an early draft.

We are indebted with two anonymous referees and with the editors Prof. A. Mottana and Prof. A. Peccerillo for the useful suggestions.

References

Antelo, J., Avena, M., Fiol, S., López, R., Arce, F. (2005): Effects of pH and ionic strength on the adsorption of phosphate and arsenate at the goethite-water interface. *J. Colloid Interface Sci.*, **285**, 476-486.

Cheinost, A.C. & Schwertmann, U. (1999): Color Identification of Iron Oxides and Hydroxysulfates: use and Limitation. *Soil Sci. Soc. Am. J.*, **63**, 1463-1471.

Cornell, R.M. & Schwertmann, U. (2003): The iron oxides. Structure, properties, reactions, occurrence and uses. 2nd ed. Wiley-VCH, Weinheim, Germany, 663 p.

Dixit, S. & Hering, J. (2003): Comparison of arsenic (V) and arsenic (III) sorption onto iron oxide minerals: implications for arsenic mobility. *Environ. Sci. Technol.*, **37**, 4182-4189.

Dzombak, D.A. & Morel, F.M. (1990): Surface complexation modelling: hydrous ferric oxide. John Wiley & Sons, New York, 331 p.

Fei, A. (1997): Le preziose "terre" di Arcidosso e Castel del Piano (Grosseto). *Atti Museo Storia Nat. Grosseto*, **16**, 141-162.

Fendorf, S., Eick, M., Grossl, P., Sparks, D. (1997): Arsenate and chromate retention mechanism on goethite. 1- Surface structure. *Environ. Sci. Technol.*, **31**, 315-320.

Ferrari, L., Ponticelli, S., Burlamacchi, L., Manetti, P. (1996): Volcanological evolution of the Monte Amiata, southern Tuscany: new geological and petrochemical data. *Acta Vulcanol.*, **8**, 41-56.

Fuller, C., Davis, J., Waychunas, G. (1993): Surface chemistry of ferrihydrite: part 2. Kinetics of arsenate adsorption and coprecipitation. *Geochim. Cosmochim. Acta*, **57**, 2271-2282.

Gao, Y. & Mucci, A. (2001): Acid base reactions, phosphate and arsenate complexation, and their competitive adsorption at the surface of goethite in 0.7 M NaCl solution. *Geochim. Cosmochim. Acta*, **65**, 2361-2378.

Garcia-Sanchez, A., Alvarez-Ayuso, E., Rodriguez-Martin, F. (2002): Sorption of As (V) by some oxyhydroxides and clay minerals. Application to its immobilization in two polluted mining soils. *Clay Miner.*, **37**, 187-194.

Gasperini, G. (1906): La fitogenesi delle terre rosse, gialle e bolari e la importanza delle Beggiatoaceae per la circolazione e deposizione del ferro. *Atti R. Accad. Georg., Ser.* 5, **3**, 503-572.

Giannetti, C. (1873): Sulle terre gialle e bolari del Monte Amiata con appendice relativa alla farina fossile del Monte Amiata. Lazzeri, Siena.

Gräfe, M., Eick, M.J., Grossl, P.R. (2001): Adsorption of arsenate (V) and arsenite (III) on goethite in the presence and absence of dissolved organic carbon. *Soil Sci. Soc. Am. J.*, **65** (*6*), 1680-1687.

Grossl, P.R., Eick, M., Sparks, D.L., Goldberg, S., Ainsworth, C.C. (1997): Arsenate and chromate retention mechanisms on goethite. 2. Kinetic evaluation using a pressure-jump relaxation technique. *Envrion. Sci. Technol.*, **31**, 321-326.

Gualtieri, A.F. & Venturelli, P. (1999): *In situ* study of the goethite-hematite phase transformation by real time synchrotron powder diffraction. *Am. Mineral.*, **84**, 895-904.

Harley, R.D. (1982): Artists' Pigments c. 1600-1835. Butterworths Scientific, London.

Helwig, K. (1997): A note on burnt yellow earth pigments: documentary sources and scientific analysis. *Stud. Conserv.*, **42**, 181-188.

Hiemstra, T. & Van Riemsdijk, W.H. (1999): Surface structural ion adsorption modeling of competitive binding of oxyanions by metal (hydr)oxides. *J. Coll. Interface Sci.*, **210**, 182-193.

Hingston, F.J., Posner, A.M., Quirk, J.P. (1971): Competitive adsorption of negatively charged ligands on oxide surfaces. *Discuss. Faraday Soc.*, **52**, 334-342.

Lotti, B. (1910): Geologia della Toscana. *Mem. Descr. Carta Geol. d'Italia.*, **XIII**, 482 p.

Manasse, E. (1915): Sulla composizione chimica delle terre gialle e bolari del Monte Amiata. *Atti Soc. Tosc. Sci. Nat., Mem.*, **XXX**, 101-119.

Manning, B.A. & Goldberg, S. (1996): Modeling competitive adsorption of arsenate with phosphate and molybdate on oxide minerals. *Soil Sci. Soc. Am. J.*, **60**, 121-131.

Manning, B.A., Fendorf, S.E., Goldberg, S. (1998): Surface structures and stability of arsenic (III) on goethite: Spectroscopic evidence for inner-sphere complexes. *Environ. Sci. Technol.*, **32**, 2383-2388.

Moretti, A. (1937): Le terre coloranti italiane. *Ind. Miner.*, **11**, 155-168.

Myneni, S., Traina, S., Waychunas, G., Logan, T. (1998): Experimental and theoretical spectroscopic evaluation of arsenate coordination in aqueous solutions, solids, and at mineral-water interfaces. *Geochim. Cosmochim. Acta*, **62**, 3285-3300.

O'Reilly, S.E., Strawn, D.G., Sparks, D.L. (2001): Residence time effects on arsenate adsorption / desorption mechanisms on goethite. *Soil Sci. Soc. Am. J.*, **65**, 67-77.

Pomies, M.P., Morin, G., Vignaud, C. (1998): XRD study of the goethite-hematite transformation: application to the identification of heated prehistoric pigments. *Eur. J. Solid State Inorg. Chem.*, **35**, 9-25.

Pomies, M.P., Menu, M., Vignaud, C. (1999): TEM observation of goethite dehydration: application to archaeological samples. *J. Eur. Ceram. Soc.*, **19**, 1605-1614.

Ruan, H.D., Frost, R.L., Kloprogge, J.T., Duong, L. (2002): Infrared spectroscopy of goethite dehydroxylation: III. FT-IR microscopy of in situ study of thermal transformation of goethite to hematite. *Spectrochim. Acta A*, **58**, 967-981.

Scarzella, P. & Natale, P. (1989): Terre coloranti naturali e tinte murali a base di terre. Monografie e catalogo delle collezioni di terre coloranti e di campioni di coloriture a base di terre allestite al Politecnico di Torino. *Stamperia Artistica Nazionale*, Torino.

Sherman, D.M. & Randall, S.R. (2003): Surface complexation of arsenic (V) to iron (III) (hydr)oxides: Structural mechanism from ab initio molecular geometries and EXAFS spectroscopy. *Geochim. Cosmochim. Acta*, **67**, 4223-4230.

Smedley, P.L. & Kinniburgh, D.G. (2002): A review of the source, behaviour and distribution of arsenic in natural waters. *Appl. Geochem.*, **17**, 517-568.

Sun, X. & Doner, H.E. (1996): An investigation of arsenate and arsenite bonding structures on goethite by FTIR. *Soil Sci.*, **161**, 865-872.

Walter, D., Buxbaum, G., Laqua, W. (2001): The mechanism of the thermal transformation from goethite to hematite. *J. Therm. Anal. Cal.*, **63**, 733-748.

Waychunas, G.A., Rea, B.A., Fuller, C.C., Davis, J.A. (1993): Surface chemistry of ferrihydrite: Part 1. EXAFS studies of the geometry of coprecipitated and adsorbed arsenate. *Geochim. Cosmochim. Acta*, **57**, 2251.

Waychunas, G.A., Davis, J.A., Fuller, C.C. (1995): Geometry of sorbed arsenate on ferrihydrite and crystalline FeOOH: Revaluation of EXAFS results and topological factors in prediction sorbate geometry and evidence for monodentate complexes. *Geochim. Cosmochim. Acta*, **59**, 3655-3661.

Received 9 May 2006
Modified version received 6 September 2006
Accepted 25 September 2006